A Comparison of Tonal Noise Characteristics of Large Multicopters with Phased Rotors

Brendan Smith*
PhD Student

Farhan Gandhi
Redfern Chair, Director

Robert Niemiec
Research Scientist

Center for Mobility with Vertical Lift (MOVE)
Rensselaer Polytechnic Institute Troy, New York, United States

This study examines the acoustic behavior in hover of manned -size, multirotor, eVTOL aircraft in the classical quadcopter, hexacopter, and octocopter configurations. The rotors are assumed to have collective pitch control and operate at a specified RPM, with orthogonal and tip-to-tip rotor phasing considered. All configurations have the same disk loading and tip Mach number, with the rotor radius decreasing and RPM increasing, going from the quadcopter to the octocopter. The simulations use the Rensselaer Multicopter Analysis Code for the aerodynamic loads on the blades, coupled to an acoustic propagation code for noise predictions at selected observer locations. From the simulation results, orthogonal phasing between rotors is shown to produce significant noise reductions along interboom bisectors (between 9 and 14 dB relative to an equivalent single rotor, at 6 lb/ft^2 disk loading and 0.51 tip Mach number). Further reducing the tip Mach number not only reduces the propagated noise but produces even deeper regions of quiet along the interboom bisectors (18–25 dB quieter at 3 lb/ft^2 with 0.36 tip Mach number). An examination of the sound pressure level frequency spectra indicates that smaller faster spinning rotors (going from the quadcopter to octocopter) produce more tonal peaks at higher frequencies which would result in penalties in A-weighted noise.

Introduction

With the emergence of distributed electric propulsion as a key enabling technology viable at a larger scale, there has been tremendous interest in recent years in the development of multirotor electric vertical takeoff and landing (eVTOL) aircraft. While battery-powered, electric motor-driven, small multicopters have been available to hobbyists, videographers, and recreational users for quite some time, there is now a strong push toward the development of *manned-size* eVTOL aircraft in support of the urban air mobility (UAM) vision, as promoted through the likes of the Uber Elevate Program (Ref. 1), the NASA UAM Grand Challenge (Refs. 2, 3), and the establishment of many strategic partnerships and a UAM ecosystem. The success of the UAM vision, relying on the ubiquitous use of manned-size eVTOL aircraft to quickly and efficiently ferry people and goods across the urban/suburban landscape, however, requires overcoming several major technical and logistical challenges.

Key among the technical challenges is the noise generated by eVTOL aircraft operating in areas of high population density and its impact on community acceptance. Sustained work over the last several decades has resulted in an excellent understanding of the aeroacoustic characteristics of conventional helicopters. For example, Ref. 4 explains the key noise sources—thickness noise, loading noise, high-speed impulsive noise, and blade–vortex interaction noise—on conventional helicopters and the conditions in which they dominate. However, a similar degree of understanding is currently lacking for multirotor eVTOL aircraft.

To address this gap, the Aeroacoustics Branch at NASA Langley Research Center has undertaken a significant campaign focusing on experimental studies as well as associated simulations and analysis on small, fixed-pitch, variable-RPM rotors, and their assemblies (Refs. 5–10). Their studies examine, in detail, the noise-contributing sources, rotor–airframe interaction effects, broadband noise, and the effect of phase synchronization between rotors. Reference 8 looked at the cancellation effects of phasing on rotor pairs and then applied this to an octocopter to examine the benefits gained on a vehicle level. Additional studies of acoustic measurements on small, fixed-pitch, variable-RPM single rotors, quadcopters, and hexacopters, recently conducted by other academic groups, are reported in Refs. 11–13.

Several simulation studies on acoustics of multirotor aircraft have also been conducted in recent years. Unlike the experimental studies in the previous paragraph on small rotors, many of these simulations focus on larger multirotor aircraft with a direct relevance to UAM applications and missions. Passe and Baeder (Ref. 14) studied the effect of rotor design parameters and boom shadow on eVTOL aeroacoustic characteristics in hover conditions. Quackenbush et al. (Ref. 15) and Jia and Lee (Ref. 16) analyzed the acoustic characteristics of very specific configurations currently under study in the eVTOL community, such as Piasecki's slowed rotor wing-compounded eVTOL design, and NASA's one- and six-passenger concept quadrotor eVTOL designs. Another area that is receiving much attention lately is the aeroacoustic implications of propeller–wing, –body, –duct, and –boom interactions (Refs. 14, 17–19) likely to be encountered on typical eVTOL aircraft. Similarly, there is high interest in broadband noise of variable-RPM eVTOL rotors (Refs. 7, 20–23), since this has been identified to be a

*Corresponding author; email: smithb12@rpi.edu.
Manuscript received January 2022; accepted December 2022.

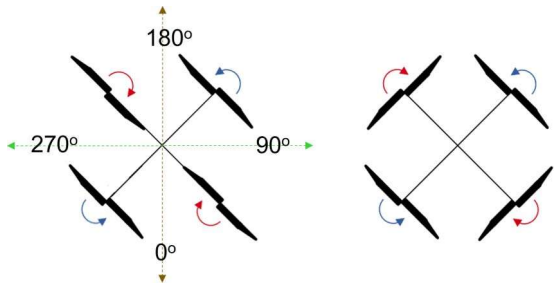

Fig. 1. Quadcopter with orthogonal (left) and tip-to-tip (right) rotor phasing.

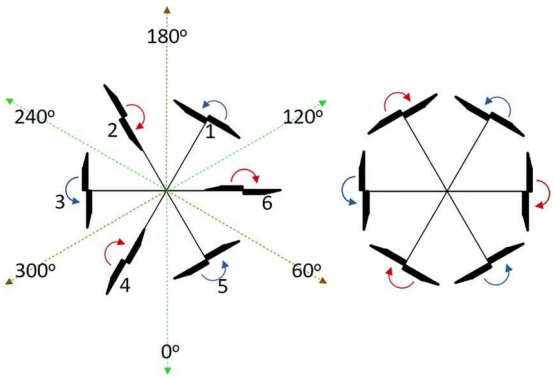

Fig. 2. Hexacopter with orthogonal (left) and tip-to-tip (right) rotor phasing.

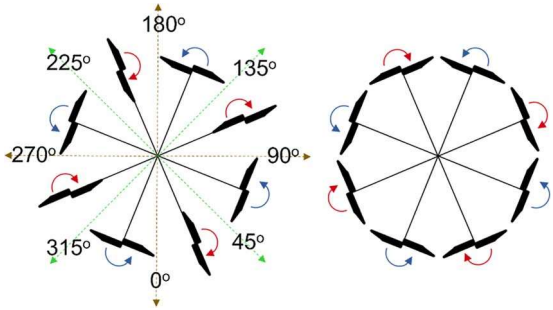

Fig. 3. Octocopter with orthogonal (left) and tip-to-tip (right) rotor phasing.

more important noise source than seen on traditional helicopter rotors (Refs. 5, 10).

There are also other factors to consider in eVTOL aircraft development that can ultimately have implications on aeroacoustics. While nearly all small multicopters are controlled using variable-RPM rotors, recent studies suggest that, as the rotor diameter increases, variable-RPM control alone will result in significant motor weight penalty to meet handling qualities requirements, with particularly heavy motors needed to meet piloted bandwidth requirements (Refs. 24–27). Collective pitch control on individual rotors offers one solution to this challenge, and as an example, Joby Aviation's four-passenger S4 aircraft (Ref. 28) includes this feature. The presence of collective pitch control, in turn, allows for potential phase synchronization between various rotors operating at the same speed. References 29 and 30 have already explored the use of rotor phasing for eVTOL aircraft vibration reduction, and there is also the potential to further develop on the ideas in Refs. 8 and 9 for improved aeroacoustics of large eVTOL aircraft. Beyond the academic and government research groups, even OEMs (original equipment manufacturers) are seriously considering the acoustic benefits of phase synchronization as seen in patent applications by Bell Helicopters and Joby Aviation (Refs. 30, 31).

With this background, the current study examines the aeroacoustic characteristics of UAM-scale, multirotor eVTOL aircraft in hover, specifically comparing the influence of the number of rotors and variation in disk loading (through change in tip Mach number or rotor root pitch) on noise levels and radiated acoustic energy. With each rotor operating at the same RPM, the effect of rotor-to-rotor phasing is considered and the study places a strong emphasis on understanding the interference behavior from multiple coherent acoustic sources, which the individual rotors present.

Analysis

The rotor aerodynamic loads for the multirotor configurations considered in the present study are evaluated using the Rensselaer Multicopter Analysis Code (RMAC), a physics-based comprehensive and flight-simulation analysis tool described in Ref. 32. RMAC uses blade-element theory, in conjunction with a 10-state Peters–He finite-state dynamic wake model to calculate the blade sectional aerodynamic loads which can be integrated along the span and around the azimuth to obtain the rotor loads. While RMAC has the capability to model the rotor blades as rigid or undergoing elastic deformation, the rigid blade option is exercised in the current simulations. Rotor–rotor interactional aerodynamic effects, which are negligible in hover, are not considered in the present study

Three different multicopter configurations—a classical quadcopter, a classical hexacopter, and a classical octocopter—each with two-bladed rotors, are considered in hover conditions. Two different rotor phasing scenarios for each multicopter are examined, as shown in Figs. 1–3. With *orthogonal phasing*, the blade-tip to blade-tip distance between adjacent rotors is a maximum, while *tip-to-tip phasing* results in that distance being a minimum. As the figures indicate, tip-to-tip phasing has the blades of each rotor positioned normal to their corresponding boom axis at the same instant during every revolution. With orthogonal phasing, when alternate rotors (say the counterclockwise rotors) have their blades positioned normal to their booms, the adjacent rotors (the clockwise rotors) have their blades aligned along their booms at the same instant during every revolution.

To enable fair comparisons across the multicopter configurations, the nondimensional rotor geometric parameters and airfoils are identical (rotor solidity of 0.0646, blade linear twist of –12 deg/span, linear taper with a tip chord/root chord of 0.75, and a linear blend of airfoils from a NACA 2412 at the blade root to a Clark Y at the tip). The nominal aircraft gross weight is 1206 lb, and the nominal blade root pitch (to achieve the required thrust to hover) is 18.8 deg, across multicopter configurations. The total disk area across configurations is the same (maintaining a nominal disk loading of 6 lb/ft^2), so the rotor radius progressively decreases going from the quadcopter to the octocopter. The boom length for each configuration is set such that the tip clearance between the rotors is 10% of the rotor's radius. The tip Mach number (nominally at 0.51) is unchanged across configurations, so the rotor RPM increases going from the quadcopter to the octocopter. Variation in rotor radius and RPM across multicopter configurations is presented in Table 1. Also considered for comparison is an *equivalent single rotor* with twice the radius of the quadcopter rotors and operating at half the RPM of the quadcopter rotors. Thus, the equivalent single rotor has the same disk loading and tip Mach number as the multicopter configurations. Its radius is denoted as R_0.

The blade loads from each rotor are provided as inputs to an acoustic propagation solver. Two different solvers, PSU-WOPWOP (Ref. 34) and ANOPP2 (Ref. 35), both of which are based on the numerical

Table 1. Rotor radius and RPM for various multicopter configurations

	Single Rotor	Quadcopter	Hexacopter	Octocopter
Radius	2.438 m (8 ft)	1.219 m (4 ft)	0.995 m (3.226 ft)	0.862 m (2.828 ft)
RPM	685.5	1371	1679	1939

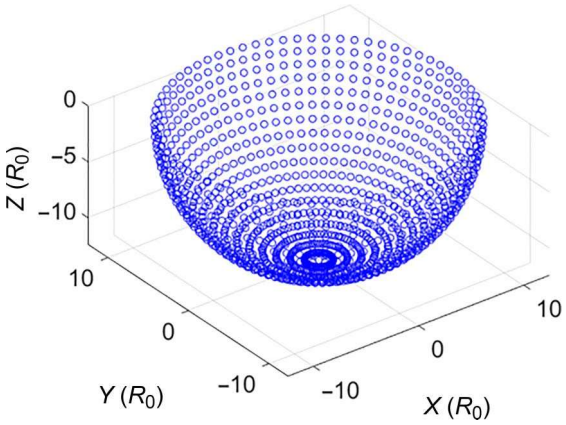

Fig. 4. Hemisphere of radius 12.5R_0, showing observer locations at 5 deg increments in azimuth and elevation angle.

implementation of Farassat's Formulation 1A of the Ffowcs Williams and Hawkings equation. Both were used and yielded the same tonal noise predictions for the same rotor loading. Broadband noise predictions were obtained using ANOPP2, which has previously shown good validation with experiments for broadband noise of small electrically powered rotors (Ref. 7). RMAC provides chordwise compact loads to the acoustic solver to compute the discrete frequency (tonal) noise from thickness and loading sources. The solver calculates the acoustic pressure time history at observer locations selected by the user, coming from the specified number of rotors (whose positions, and relative rotor phasing are also specified). In the present study, observers are placed on a 100-ft radius hemisphere (12.5 times the equivalent single rotor radius, R_o, and distant enough to be in the acoustic far-field) in 5 deg increments in both azimuth and elevation angle, as shown in Fig. 4. The overall sound pressure level (OASPL) in dB and dBA are calculated from the acoustic pressure time histories.

Along with tonal noise, the solvers can calculate broadband noise from the rotors using additional information from the rotors provided by RMAC. The broadband noise will be the dominant noise source at higher frequencies, which can be seen in Figs. 5(a) and 5(b) which gives the sound pressure level as a function of frequency for the quadcopter in orthogonal and tip-to-tip phasing at an observer in plane, in front of the vehicle ($\Psi = 180^\circ$). The broadband noise becomes the dominant noise source at frequencies greater than 600 Hz, with tonal peaks of much greater magnitude being dominant below this range. Of note is the fact that the magnitude of the tonal peaks at lower frequencies, while dependent on the relative rotor phasing used, is unchanged whether or not broadband noise is included in the computation. Since this study is focused on the effects of phasing on the noise, broadband noise will not be considered for the results shown in the remainder of the paper, with only tonal noise calculations presented.

Also calculated, for comparison across various configurations, is the total acoustic power radiated (PWL) over the observer hemisphere. First, the sound intensity normal to the individual observers is calculated from the acoustic pressure time history using

$$I = \frac{p^2}{\rho c} \tag{1}$$

where p^2 is the mean square pressure at the observer, ρ is the air density, and c is the speed of sound.

The radiated acoustic power (PWL), for any configuration, is obtained by integrating the sound intensity calculated above over the surface of the hemisphere. However, the radiated acoustic power results presented in the current study are normalized with respect to the equivalent single rotor as follows:

$$\mathrm{PWL_{dB}} = 10 * \log_{10}\left(\frac{\mathrm{PWL_{multicopter}}}{\mathrm{PWL_{equivalent\ single\ rotor}}}\right). \tag{2}$$

Validation

The present simulation method (with RMAC blade load predictions coupled to the acoustic propagation code described in the second section) is first validated against experimental and simulation results from NASA Langley Research Center reported by Schiller et al (Ref. 8). In Ref. 8, a two-rotor system was considered, with rotors operating in both

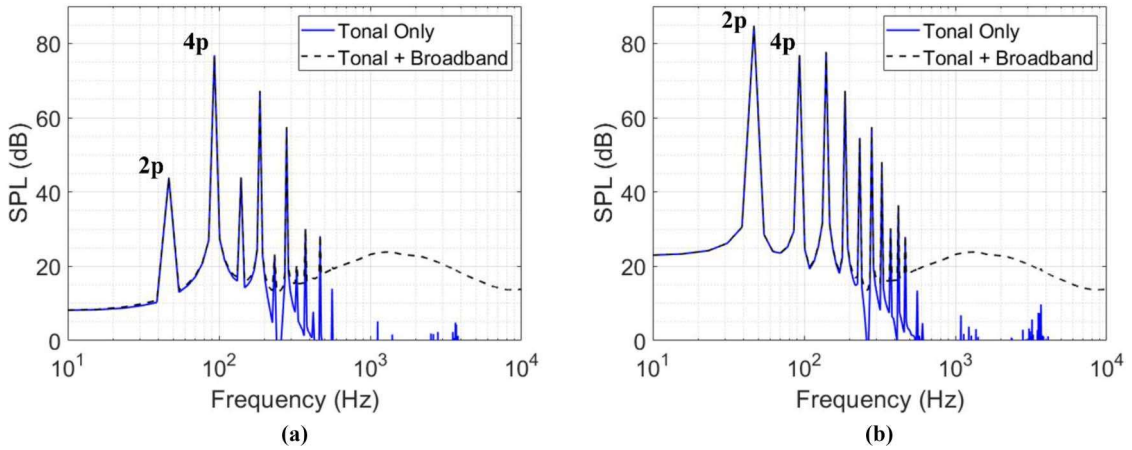

Fig. 5. SPL for quadcopter with (a) orthogonal phasing (in-plane observer at $\Psi = 180°$) (b) tip-to-tip phasing (in-plane observer at $\Psi = 180°$).

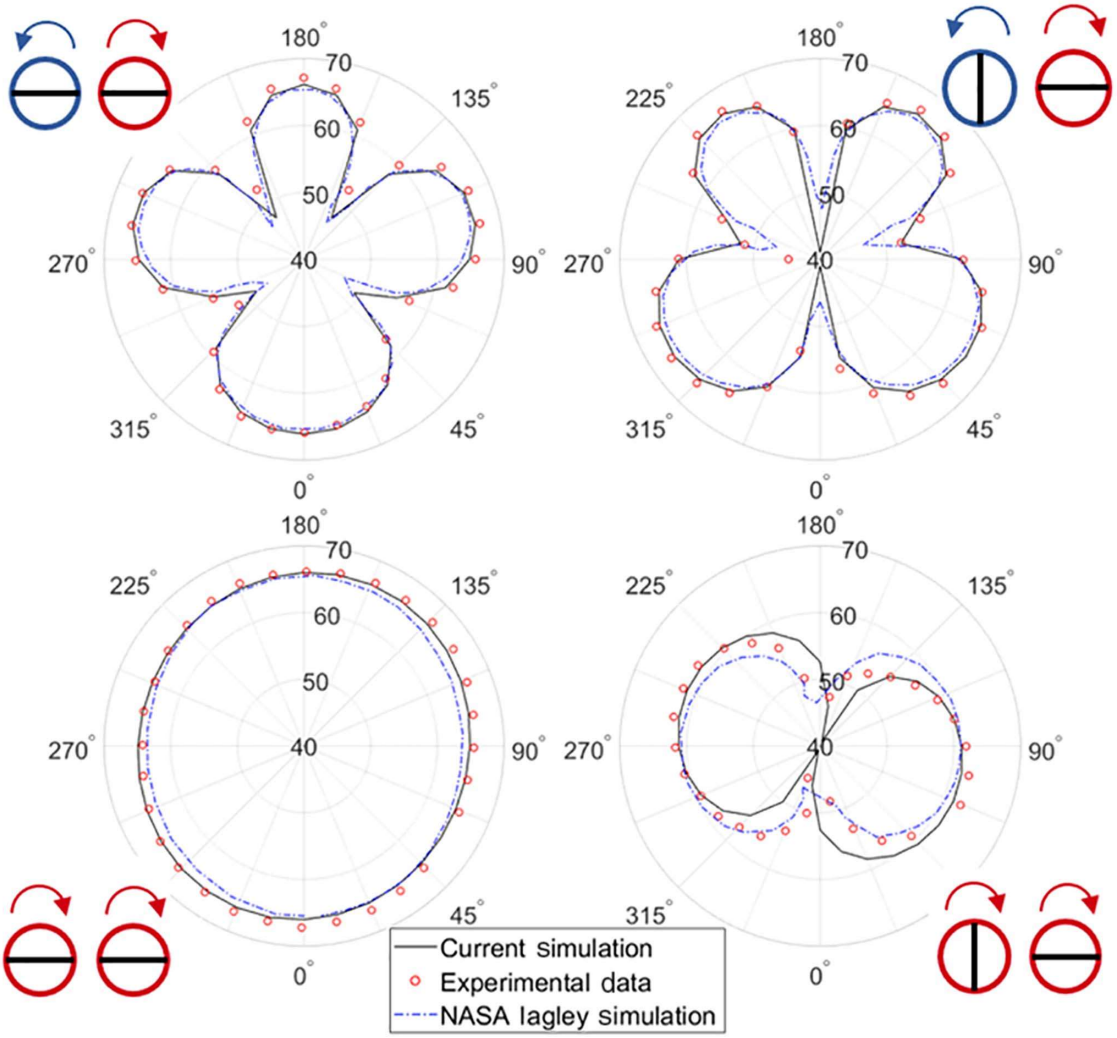

Fig. 6. Validation of sound pressure level predictions at blade passage frequency in the plane of the rotors, versus NASA Langley experiment and simulation results.

corotating and counterrotating configurations, and with a relative phasing of 0° and 90° . Each rotor was two-bladed, had a diameter of 0.317 m, and a clearance of 0.083 m between the rotor disks. Microphones were placed over a 1.9-m radius partial hemisphere at five equally spaced observer stations between elevation angles of 0° (in-plane) and –45° and moved in 11.25° increments (corresponding to 32 points) around the azimuth. Rotor operational details for the present simulation (RPM, thrust, etc.) were matched to those reported in Ref. 8. As was done with the NASA Langley experimental data, only the spectral energy within a ± 10 Hz window around the blade passage frequency was considered when evaluating the sound pressure level.

Figure 6 shows a comparison of the sound pressure level predictions in the plane of the rotors for four different cases (representing differences in direction of rotation and rotor phasing). The cloverleaf shape observed in the counterrotating pairings in the NASA experiments and simulations is captured accurately by the present simulations. The corotating pairs also match well, with the almost axisymmetric shape observed for 0° relative phasing and dipole-like shape for 90° phasing well captured. Next, predictions of acoustic power radiated through the partial hemisphere (described at the end of the previous section) are compared to results from Ref. 8. Like Ref. 8, the radiated power reported is normalized by double the intensity from an isolated single rotor with the same blade radius, and the results are presented in Table 2. The present simulations show a good correlation with the experiment and excellent correlation with the NASA Langley simulations for corotating rotor pairs (which display a large increase or decrease in radiated acoustic power, depending on relative rotor phasing). Although the radiated power for counterrotating rotors shows some difference, it should be noted that the values are very small (compared to results for the corotating rotors), indicating that the radiated acoustic power from the counterrotating pairs over the partial hemisphere is essentially very similar to twice that radiated by the single rotor operating in isolation. In summary, the validation results in Fig. 6 and in Table 2 provide good confidence in the simulation tools used in the present study.

Results

Quadcopter

Figure 1 shows a quadcopter with orthogonal and tip-to-tip rotor phasing, and Fig. 7 shows the OASPL on hemispheres of radius $12.5R_0$ for these two cases. With orthogonal phasing, large reductions in noise are observed along the interboom bisectors. The noise reductions are greatest along the rim of the hemisphere (or at 0° elevation, in the plane of the

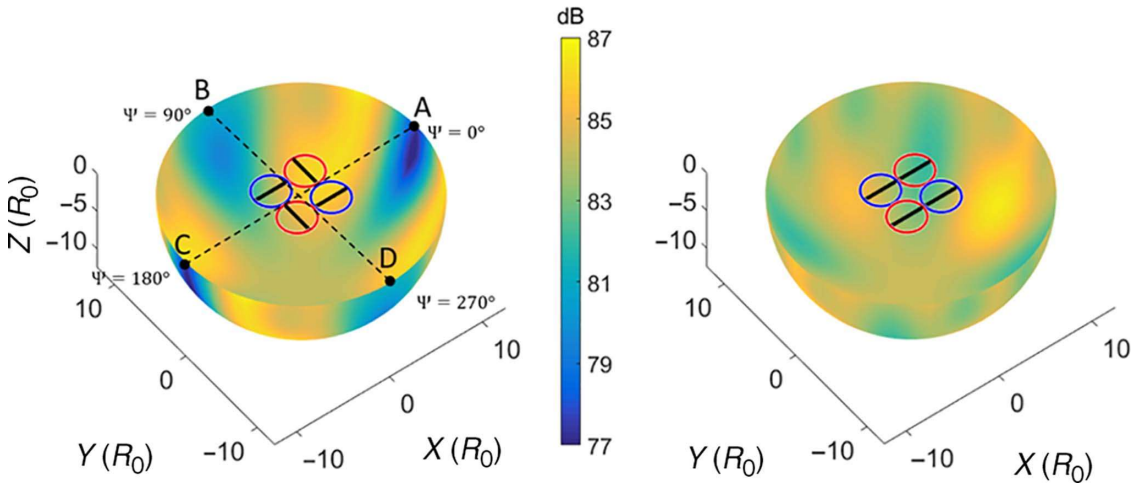

Fig. 7. OASPL for quadcopter with orthogonal (left) and tip-to-tip (right) rotor phasing (blue rotors CCW, red rotors CW).

Table 2. Radiated power over partial hemisphere for corotating and counterrotating assemblies with 0 and 90 deg phasing

Configuration	Δ PWL from Present Simulations (dB)	Δ PWL from Ref. 8 Simulations (dB)	Δ PWL from Ref. 8 Experiment (dB)
Counter, $\psi = 0°$	−0.136	0.2	0.4
Counter, $\psi = 90°$	−0.0075	−0.1	−0.3
Co, $\psi = 0°$	2.312	2.3	2.5
Co, $\psi = 90°$	−5.211	−5.2	5.8

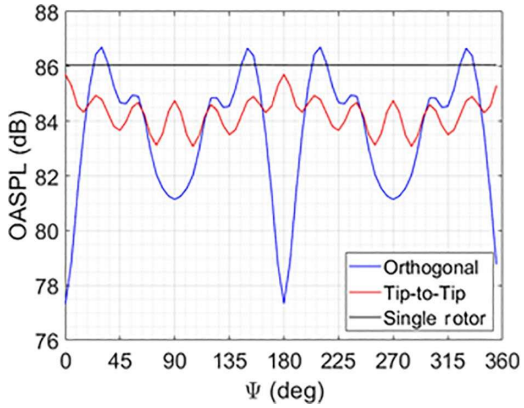

Fig. 8. OASPL comparisons at 0 deg elevation for quadcopter with orthogonal and tip-to-tip rotor phasing.

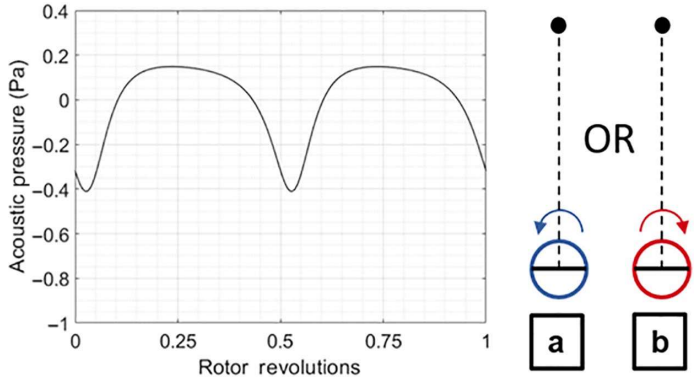

Fig. 9. Acoustic pressure at in-plane observer on the hemisphere, from a single quadcopter at the origin.

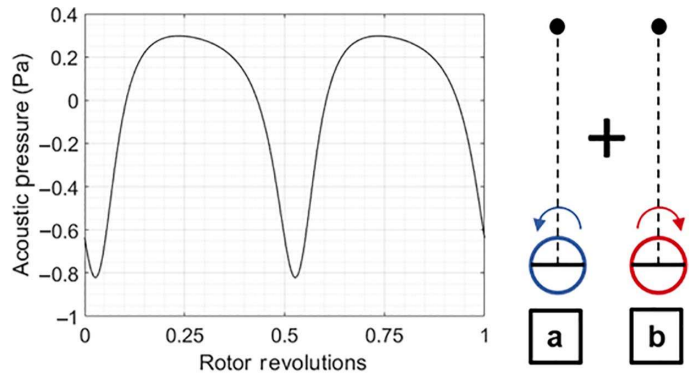

Fig. 10. Acoustic pressure at in-plane observer on the hemisphere, from coincident CW and CCW quadcopter rotors at the origin with *tip-to-tip phasing*.

rotors) and generally decrease with increasing elevation angle. Figure 8 compares the OASPL in the rotor plane (0° elevation) for the orthogonal and tip-to-tip phasing cases, with the OASPL of the single rotor also shown, as a reference. In Fig. 8, while the in-plane noise generated by the quadcopter with tip-to-tip phasing is consistently between 1 and 3 dB lower than that of the corresponding single rotor (regardless of azimuthal position), the noise along one interboom bisector for the quadcopter with orthogonal phasing is up to 9 dB lower than the single rotor. Reductions of 5 dB are observed along the other interboom bisector. The following paragraphs investigate the reasons for these differences.

Figure 9 shows the acoustic pressure signal at an in-plane observer location on the hemisphere from a single rotor of the quadcopter situated at the origin of the hemisphere. Note that counterclockwise and clockwise spinning rotors produce identical acoustic pressure signals, characterized by two negative impulsive peaks over a given rotor revolution. If a counterclockwise and a clockwise rotor, with *tip-to-tip rotor phasing*, were hypothetically superposed at the origin, the acoustic pressure peaks from each rotor would arrive at the observer at the same instant, resulting in the amplification of the individual rotor signals (Fig. 10). On the other hand, if the superposed counterclockwise and clockwise rotors are *orthogonally phased*, the acoustic pressure signals from each individual

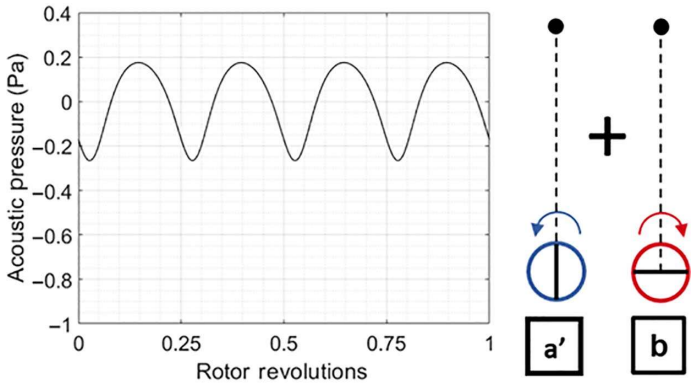

Fig. 11. Acoustic pressure at in-plane observer on the hemisphere, from coincident CW and CCW quadcopter rotors at the origin with *orthogonal phasing*.

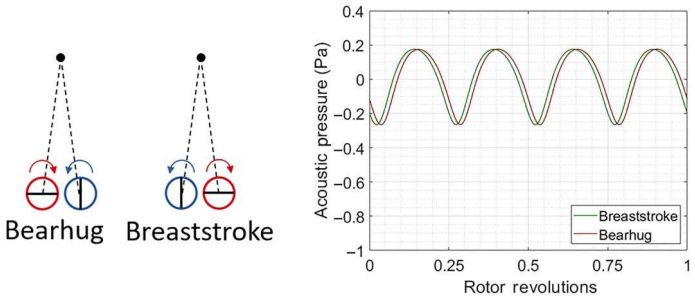

Fig. 12. Two-rotor configurations: the *bearhug* and *breaststroke*.

rotor have a quarter revolution phase difference and produce a combined signal with a 4/rev fundamental frequency (instead of 2/rev for the tip-to-tip phasing), as seen in Fig. 11.

Next, we examine the case of laterally offsetting the *orthogonally phased* coincident counterclockwise and clockwise rotors previously considered in Fig. 11. There are two possible configurations as shown in Fig. 12. The *bearhug*, where the counterclockwise rotor is offset right and the clockwise rotor offset left by an identical distance; and the *breaststroke*, where the positions are reversed. While the contributions of the individual rotors to the acoustic pressure time history at the observer are identical (other than a quarter revolution phase shift), it is to be noted that the breaststroke, with the advancing blades of both rotors closer to the observer, results in an earlier arrival of the acoustic pressure peaks. In contrast, the bearhug, with the advancing blades farther from the observer, results in a later arrival of the acoustic pressure peaks. The temporal offsets of the acoustic pressure peaks are to either side of those seen in Fig. 11 (where the counterclockwise and clockwise rotors were coincident at the origin).

In Fig. 7, counterclockwise rotors are shown in blue and clockwise rotors are shown in red. For observers A and C, the bearhugging rotor pair appears closer and the breaststroking rotor pair is situated further back. In contrast, the order is reversed for observers B and D. Figure 13 shows the acoustic pressure signal at observer A from the front bearhugging rotor pair, the rear breaststroking rotor pair, as well as the sum. The acoustic pressure peaks from the rear pair arrive later than those from the front pair (due to greater travel distance), but the temporal offset is reduced in part by the phenomena explained in Fig. 12 (that peaks from a bearhugging rotor pair arrive a little later than those from a breastroking rotor pair traveling the same distance). Similarly, Fig. 14 shows the acoustic pressure signal at observer B from the front breaststroking pair,

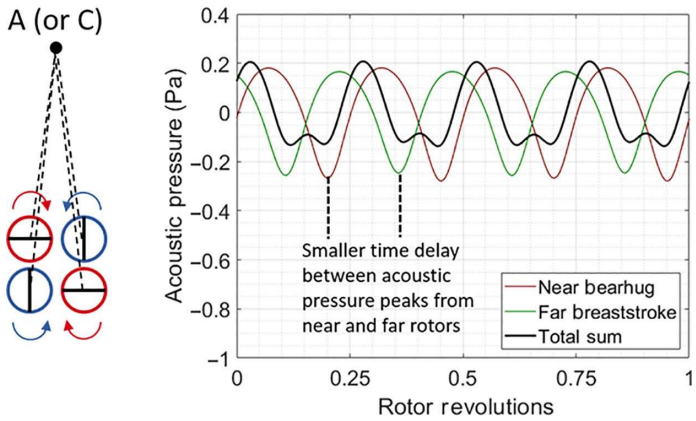

Fig. 13. In-plane acoustic pressure at points A and C on the hemisphere in Figure 7 (near *bearhug* and far *breaststroke*).

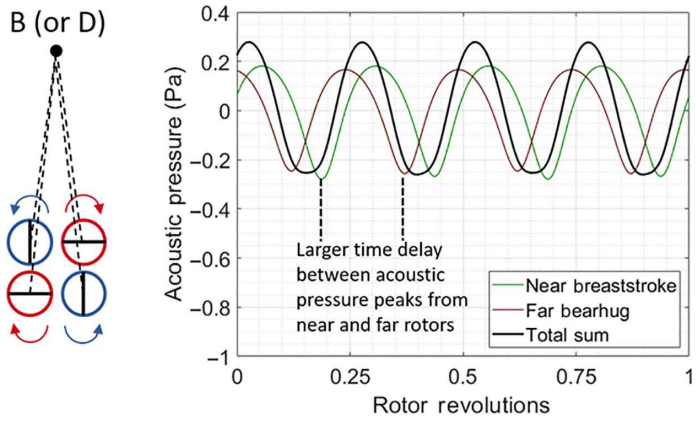

Fig. 14. In-plane acoustic pressure at points B and D on the hemisphere in Figure 7 (near *breaststroke* and far *bearhug*).

the rear bearhugging pair, and the sum. In contrast to Fig. 13, the temporal offset between the front and rear rotor acoustic pressure peaks is further increased since the front breast-stroking peaks arrive at the observer extra early, and the rear bearhugging peaks have an extra delay. The relative phasing results in a lower amplitude total acoustic pressure signal at observer A (or C), seen in the black curve in Fig. 13, compared to an observer at B (or D) (as seen in the black curve on Fig. 14). These lower amplitude acoustic waves at observers A and C (compared to B and D) in turn result in quieter regions observed in Figs. 7 and 8 for orthogonally phased rotors.

It should be noted that although the quadcopter with orthogonally phased rotors produce pronounced low-noise regions along the inter-boom bisectors (relative to rotors with tip-to-tip phasing), the integrated noise over the hemisphere is comparable to that generated over for the quadcopter with tip-to-tip phasing. Normalizing the data by that of the equivalent single rotor, the orthogonal quadcopter has PWL of −0.74 dB, and the tip-to-tip a value of −0.64 dB, showing that the net radiated power levels are close to one another for the two rotor phasing configurations.

Hexacopter and octocopter

As with the quadcopter in the previous section, the present section examines the acoustic characteristics of a hexacopter and an octocopter. Figure 2 shows a hexacopter with orthogonal and tip-to-tip rotor

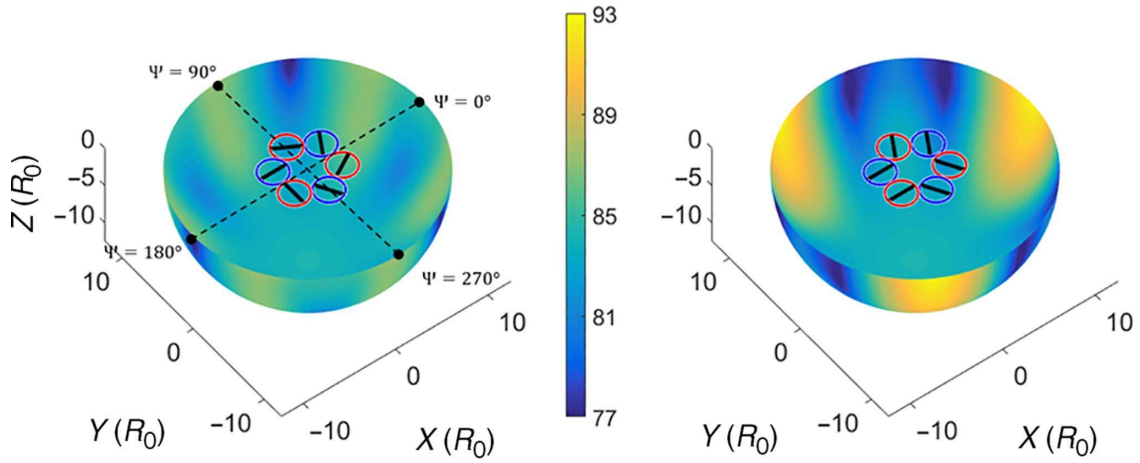

Fig. 15. OASPL for hexacopter with orthogonal (left) and tip-to-tip (right) rotor phasing (blue rotors CCW, red rotors CW),

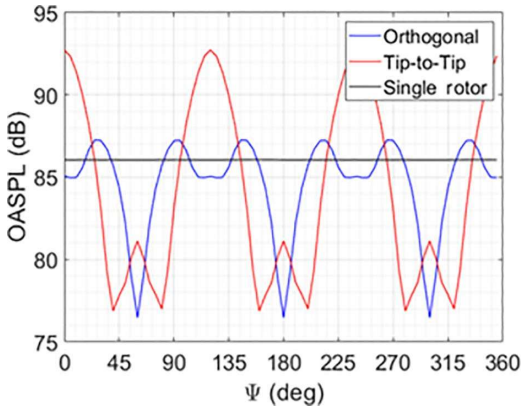

Fig. 16. OASPL comparisons at 0 deg elevation for hexacopter with orthogonal and tip-to-tip phasing.

phasing, and Fig. 13 shows the corresponding OASPL on 12.5R_0 radii hemispheres. In Fig. 15, tip-to-tip rotor phasing shows considerably higher peak noise levels than orthogonal phasing. In Fig. 7, in comparison, the quadcopter's peak noise levels did not differ appreciably between the tip-to-tip and orthogonal phasing cases, although the latter displayed regions of relative quiet along the interboom directions. Figure 16 shows the in-plane OASPL for the hexacopter (at 0° elevation, along the rim of the hemispheres). From this figure, noise reductions of up to 9.5 dB (relative to the equivalent single rotor) are observed along alternate interboom bisectors (at 60°, 180°, and 300°) in the case of orthogonal rotor phasing. From Fig. 15, it can be seen that at these quiet observer locations, the nearest rotors are a bear-hugging rotor pair. Along the other interboom bisectors (at 0°, 120°, and 240°), when the nearest rotors to the observer are a breast-stroking rotor pair, Fig. 16 shows that the noise levels are comparable to (within 1 dB of) equivalent single main rotor levels. In this regard, the hexacopter differs from the quadcopter, which showed substantial in-plane noise reductions along all interboom bisectors. From a comparison of Figs. 16 and 8, the in-plane noise of the hexacopter with tip-to-tip rotor phasing also differs substantially from that produced by the quadcopter with tip-to-tip phasing. While the tip-to-tip quadcopter showed no particular acoustic directionality in Fig. 5, the tip-to-tip hexacopter shows in-plane noise lows comparable to those of the orthogonally phased hexacopter, and along generally similar directions (see Fig. 16). Along the 0°, 120°, and 240° interboom bisectors, on the other hand, with the breast-stroking rotor pair closest to the observer, the tip-to-tip phasing produces a 7-dB noise increase over the equivalent single main rotor.

Figure 17 shows the acoustic pressure signal over a single rotor revolution along the hexacopter's 180° interboom bisector. With orthogonal rotor phasing (left figure), each rotor pair (the nearest bear-hugging pair 1–2, the intermediate breast-stroking pair 3–6, and the farthest bear-hugging pair 4–5 as denoted in Fig. 2) produces a 4/rev signal at the observer, and the relative phasing of the signals from the three rotor pairs is such that the total acoustic pressure signal has a relatively low amplitude. With tip-to-tip rotor phasing (right figure), each individual rotor pair produces a 2/rev signal at the observer, but the relative phasing once again produces a relatively low amplitude total acoustic pressure signal. Figure 18 shows similar results along the 120° interboom bisector. For orthogonal phasing, the 4/rev acoustic pressure signals from individual rotor pairs (the nearest breast-stroking pair 1–6, the intermediate bear-hugging pair 2–5, and the farthest breast-stroking pair 3-4) are relatively phased such as to generate a larger amplitude total acoustic pressure signal (compared to Fig. 17 along the 180° interboom bisector). Likewise, for tip-to-tip phasing, the 2/rev acoustic pressure signals from individual rotor pairs are relatively phased such as to generate a much larger amplitude total acoustic pressure signal (which in turn generates 7 dB higher noise than the single rotor, as seen in Fig. 16).

For the octocopters with orthogonal and tip-to-tip rotor phasing in Fig. 3, the corresponding OASPL on 12.5R_0 radii hemispheres are shown in Fig. 19. In Fig. 19, although the peak noise levels with tip-to-tip rotor phasing are comparable to those with orthogonal phasing, the tip-to-tip phasing generates significantly higher overall noise (characterized by larger areas of high noise on the hemisphere). The octocopter hemispheres show characteristics similar to those for the quadcopter in Fig. 7, with significant noise reductions along all interboom bisectors with orthogonal phasing. At 0° elevation, along the rim of the hemispheres, Fig. 20 shows 13–14 dB reductions in in-plane OASPL along the interboom directions for the orthogonal phasing case, relative to the single main rotor. For the same phasing, noise increases of up to 2.5 dB are observed along the boom directions. With tip-to-tip phasing, the octocopter generates between 2 and 4 dB higher in-plane noise, relative to the single main rotor.

Figures 21 and 22 show the acoustic pressure signals over a single rotor revolution along the octocopter's 180° and 135° interboom bisectors, respectively. With orthogonal rotor phasing (left figure), each rotor pair (starting with the nearest bear-hugging pair 1–2 for Fig. 21, and the nearest breast-stroking pair 1–8 for Fig. 22) produces a 4/rev signal at the observer, and for both observer locations, the relative phasing of the

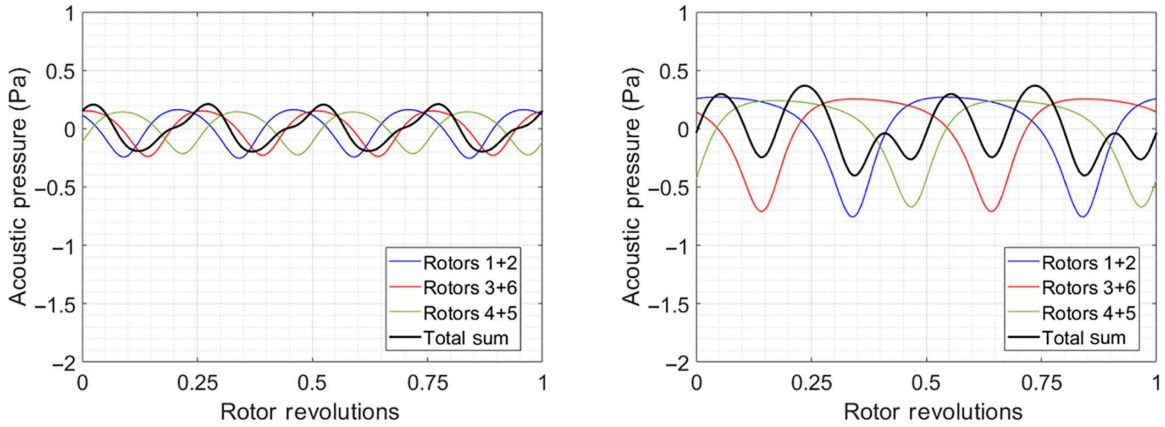

Fig. 17. Acoustic pressure at in-plane observer along the 180° interboom bisector for a hexacopter with orthogonal (left) and tip-to-tip (right) rotor phasing.

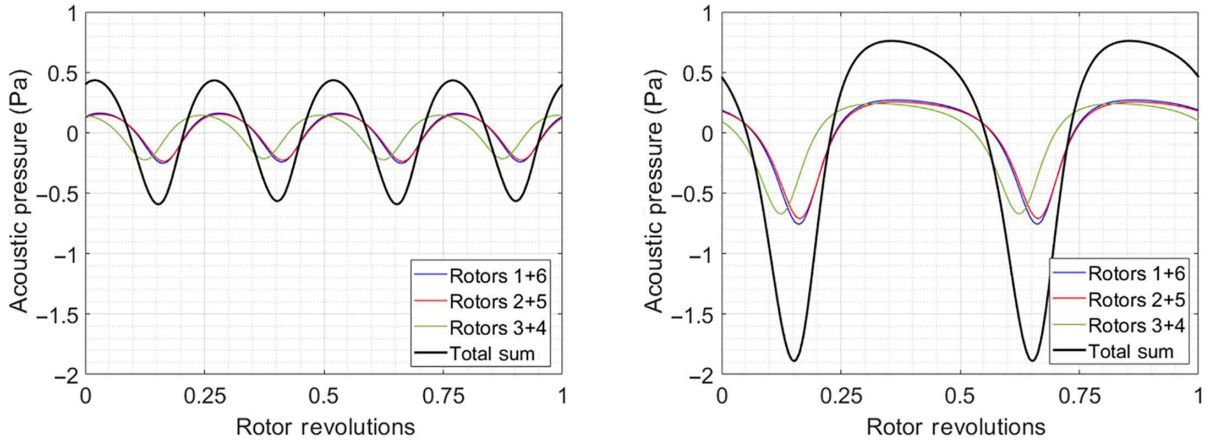

Fig. 18. Acoustic pressure at in-plane observer along the 120° interboom bisector for a hexacopter with orthogonal (left) and tip-to-tip (right) rotor phasing.

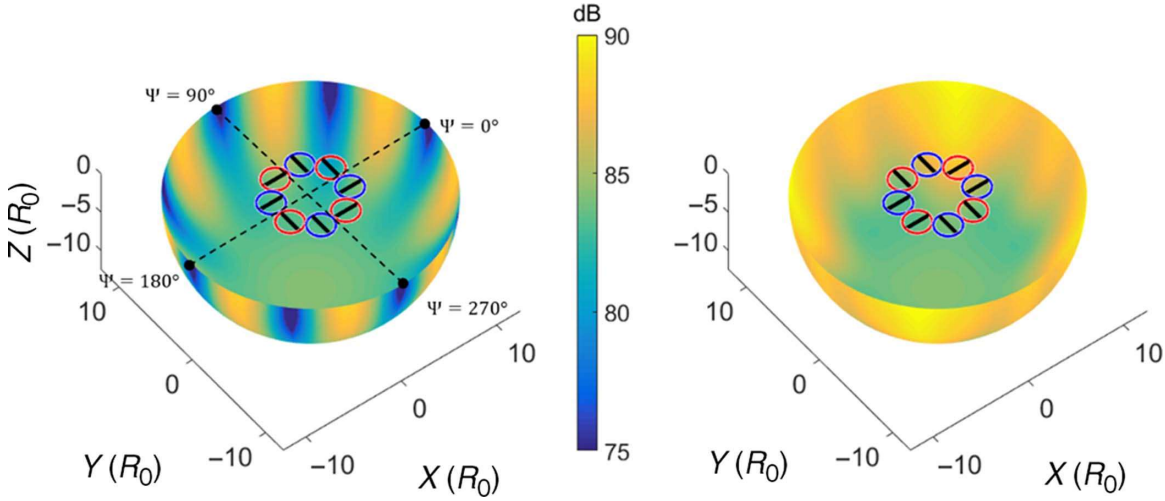

Fig. 19. OASPL for octocopter with orthogonal (left) and tip-to-tip (right) rotor phasing (blue rotors CCW, red rotors CW).

individual signals is such that the total acoustic pressure signal has a relatively low amplitude. As seen previously in the case of the hexacopter in Figs. 17 and 18, with tip-to-tip rotor phasing (right figures on Figs. 21 and 22), each individual rotor pair produces a 2/rev signal at the observer, but the relative phasing does not result in a total acoustic pressure signal of reduced amplitude (as was the case with orthogonal phasing).

Multicopter comparison

Following the results presented in the preceding subsections, the current section seeks to compare the different multicopter configurations. Figure 23 shows the frequency spectra of the sound pressure level at an in-plane observer in front of the aircraft ($\Psi = 180°$). The quadcopter,

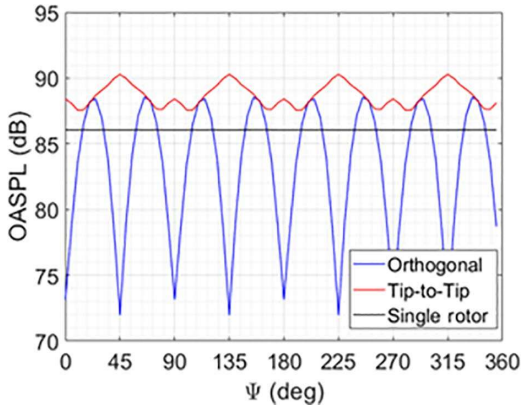

Fig. 20. OASPL comparisons at 0 deg elevation for octocopter with orthogonal and tip-to-tip rotor phasing.

hexacopter, and octocopter results in Fig. 23 are for orthogonal phasing, and in each case $\Psi = 180^{\circ}$ corresponds to an interboom direction of lowest radiated noise. As compared to the single rotor where all the tonal peaks appear to be confined to frequencies of under 300 Hz, multicopters with increasing number of smaller rotors (and correspondingly higher operating RPMs) show tonal peaks at progressively higher frequencies. Also shown in the figure is the A-weighting curve up to a frequency of 1000 Hz. Clearly, an A-weighted OASPL calculation would most penalize the octocopter (with the highest blade passage frequency of all the configurations and higher tonal peaks at higher frequencies).

Next, Table 3 presents the acoustic power radiated over the entire observer hemisphere (PWL), for the various multicopter configurations. The results, presented for both orthogonal as well as tip-to-tip phasing, are normalized with respect to the equivalent single rotor. For the quadcopter, it is interesting to note that while results in the subsection Quadcopter showed prominent regions of low noise along interboom bisectors with orthogonal phasing (absent for tip-to-tip phasing), the total radiated acoustic power over the hemisphere does not show much difference between the orthogonal and tip-to-tip phasing and is in both cases lower than the equivalent single rotor. However, this is not the case for the hexacopter and octocopter, where orthogonal phasing shows a reduction in PWL relative to the equivalent single rotor, but tip-to-tip phasing shows an increase. A –0.74 dB reduction in Table 3 for the orthogonal quadcopter represents a 15% lower PWL, while a +2.02 dB increase for the tip-to-tip octocopter represents a 59% higher PWL, relative to the equivalent single rotor.

Variation in disk loading

While the previous sections presented acoustics results for multicopters at a 6-lb/ft^2 disk loading, the present section examines the effect of change in disk loading on the acoustic characteristics of the

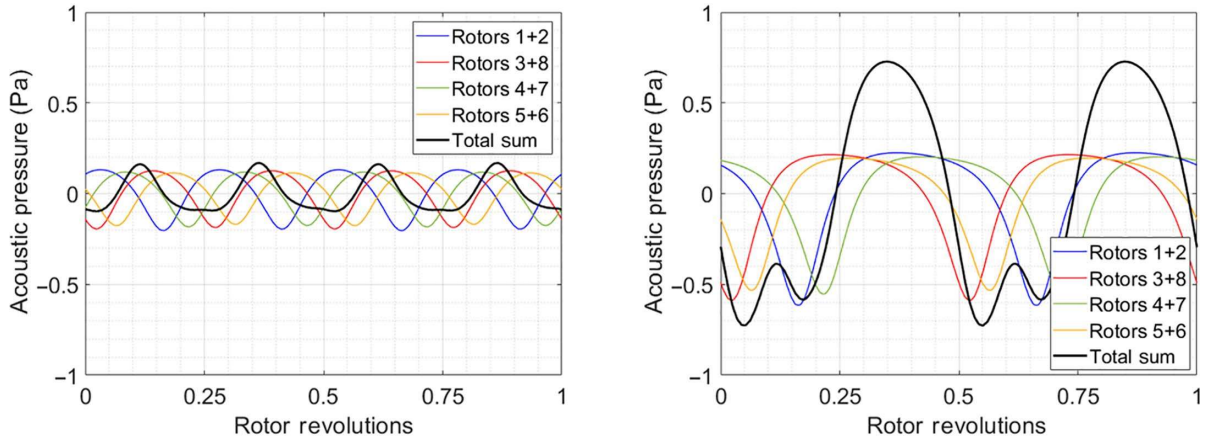

Fig. 21. Acoustic pressure at in-plane observer along the 180° interboom bisector for an octocopter with orthogonal (left) and tip-to-tip (right) rotor phasing.

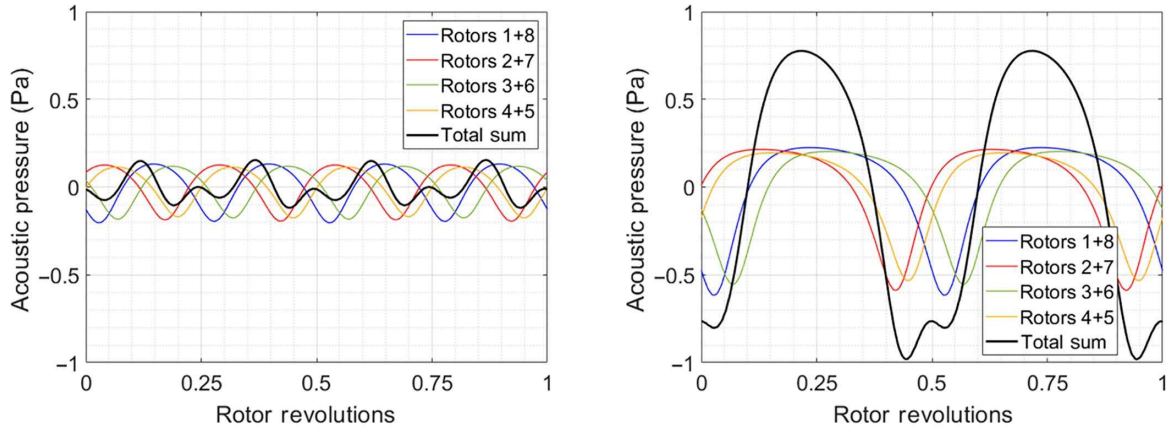

Fig. 22. Acoustic pressure at in-plane observer along the 135° interboom bisector for an octocopter with orthogonal (left) and tip-to-tip (right) rotor phasing.

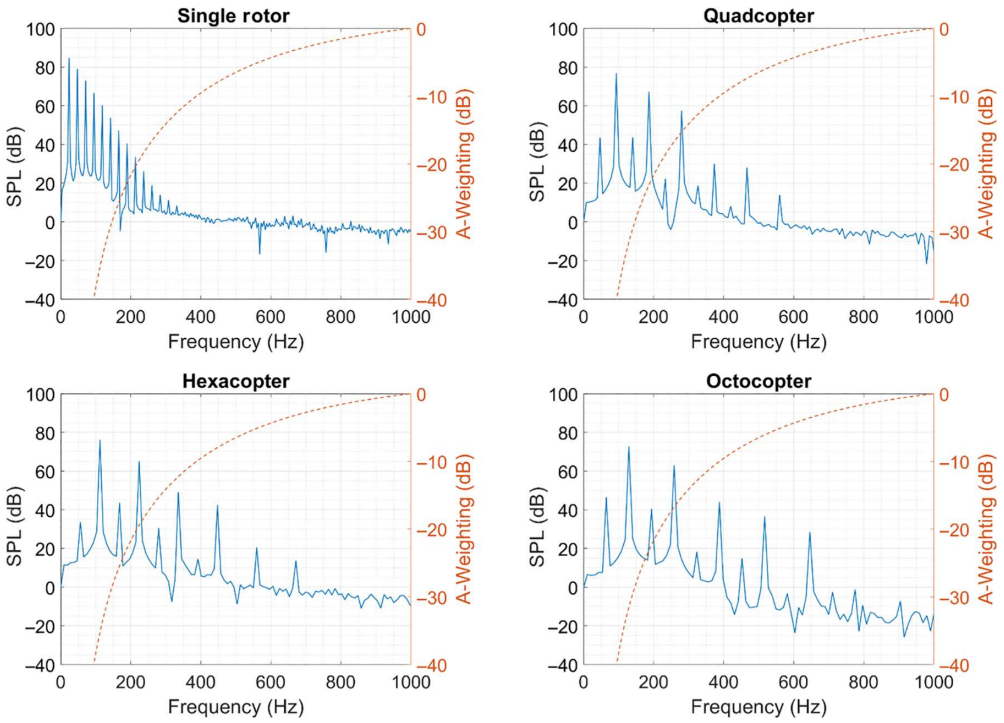

Fig. 23. A comparison of frequency spectra of sound pressure levels for various multicopter configurations.

Table 3. Acoustic power radiated over the observer hemisphere (PWL) for the various multicopter configurations relative to the single rotor

	Orthogonal (dB)	Tip-to-Tip (dB)
Quadcopter	−0.74	−0.64
Hexacopter	−0.30	1.04
Octocopter	−0.70	2.02

quadcopter. The quadcopter rotor geometry is unchanged from that described in the second section, and its radius held fixed at 4 ft as reported in Table 1. The disk loading is changed either through variation of tip speed or through variation of root pitch. Figure 24 shows contours of constant disk loading, as a function of tip Mach number and geometric root pitch. Five specific points in Fig. 24 are considered for comparison. Point A (with tip Mach number of 0.51 and root pitch of 18.8 deg) was already extensively examined in subsection Quadcopter. Points B and C correspond to rotors with the same root pitch operating at increased tip Mach numbers of 0.6 and 0.685, respectively, with corresponding disk loading values of 9 and 12 lb/ft^2. Points D and E correspond to a tip Mach number of 0.6, with root pitch values of 15.9 deg and 22.5 deg. Points D, B, and E, as a set, represent an increase in disk loading from 6 to 9 to 12 lb/ft^2, through increase in blade root pitch while holding the tip Mach number constant. An additional point, F, is considered along with the set A, B, and C, where the tip Mach number is further reduced to 0.36 to realize a disk loading of 3 lb/ft^2 disk (while holding root pitch at the nominal value of 18.8 deg, as with points A, B, and C).

Figure 25 shows the in-plane OASPL for the points F, A, B, and C in Fig. 24. Also shown in the figures is the noise generated by an equivalent single main rotor. Note that the single main rotor's tip speed on each of the plots is varied to be equal to that of the corresponding quadcopter. The noise directionality (with interboom lows) previously observed for the orthogonally phased quadcopter at 6 lb/ft^2 is not evident at the higher disk loading values (9–12l b/ft^2). At 9 lb/ft^2, the quadcopter

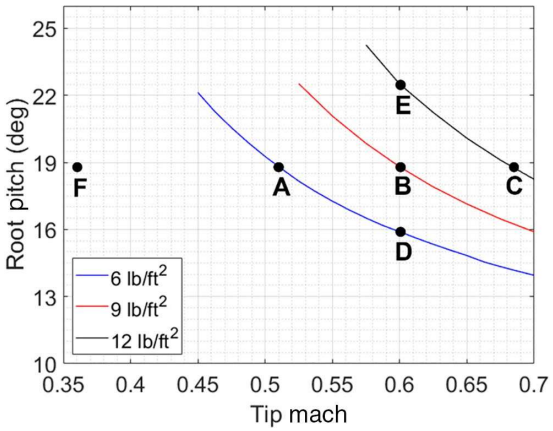

Fig. 24. Variation of disk loading with tip Mach number and root pitch.

in-plane OASPL falls within 3 dB of the single main rotor, for both rotor phasing cases considered. Similarly, at 12 lb/ft^2 in-plane OASPL values lie between –3 and +1.5 dB of the single rotor levels. At the low 3 lb/ft^2 disk loading, however, the noise directionality with orthogonal phasing is even stronger than observed at the moderate 6 lb/ft^2 loading, with the OASPL along the interboom bisectors between 18 and 25 dB lower than the single rotor. In addition to the orthogonally phased quadcopter's noise directionality (stronger at lower disk loadings) or lack thereof (at higher disk loading), the in-plane noise level, itself, rises significantly when disk loading is increased through increase in tip Mach number. Specifically, the single rotor in-plane OASPL increases from 72 dB at 3 lb/ft^2 (with tip Mach number 0.36), to 86 dB at 6 lb/ft^2 (with tip Mach number 0.51) to 92 dB at 9 lb/ft^2 (with tip Mach number 0.6) to 98 dB as the disk loading increases to 12 lb/ft^2 (at tip Mach number 0.685), with the quadcopter peak noise levels comparable to the single rotor at the same disk loading.

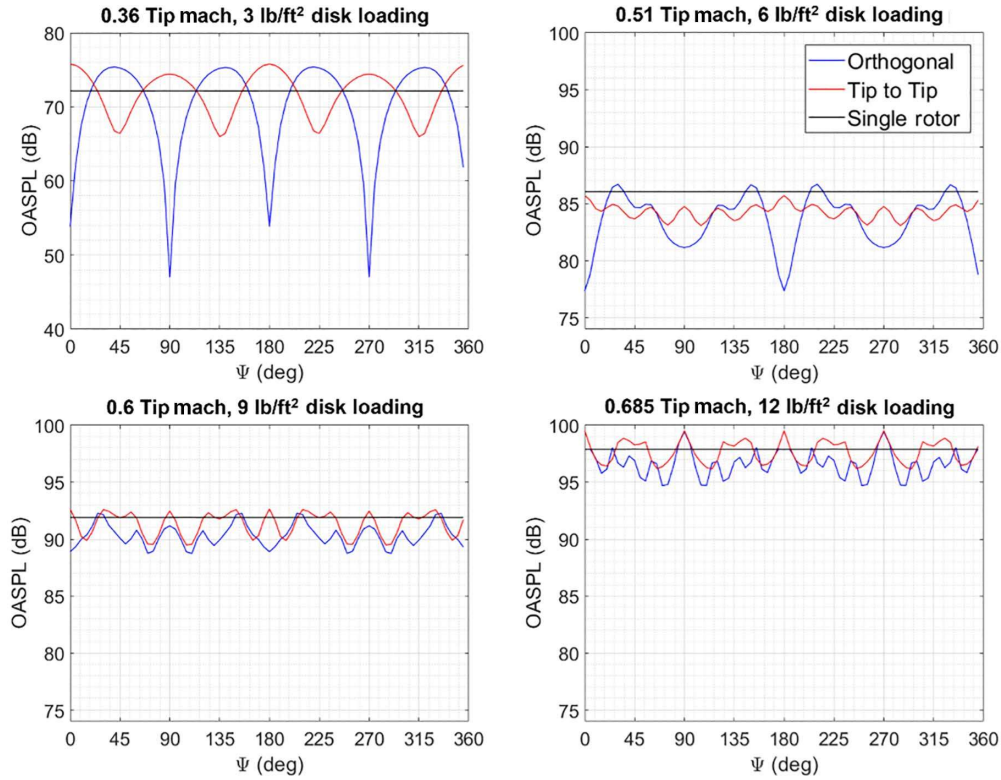

Fig. 25. In-plane OASPL for increasing disk loading with increasing tip Mach number (constant root pitch of 18.8 deg).

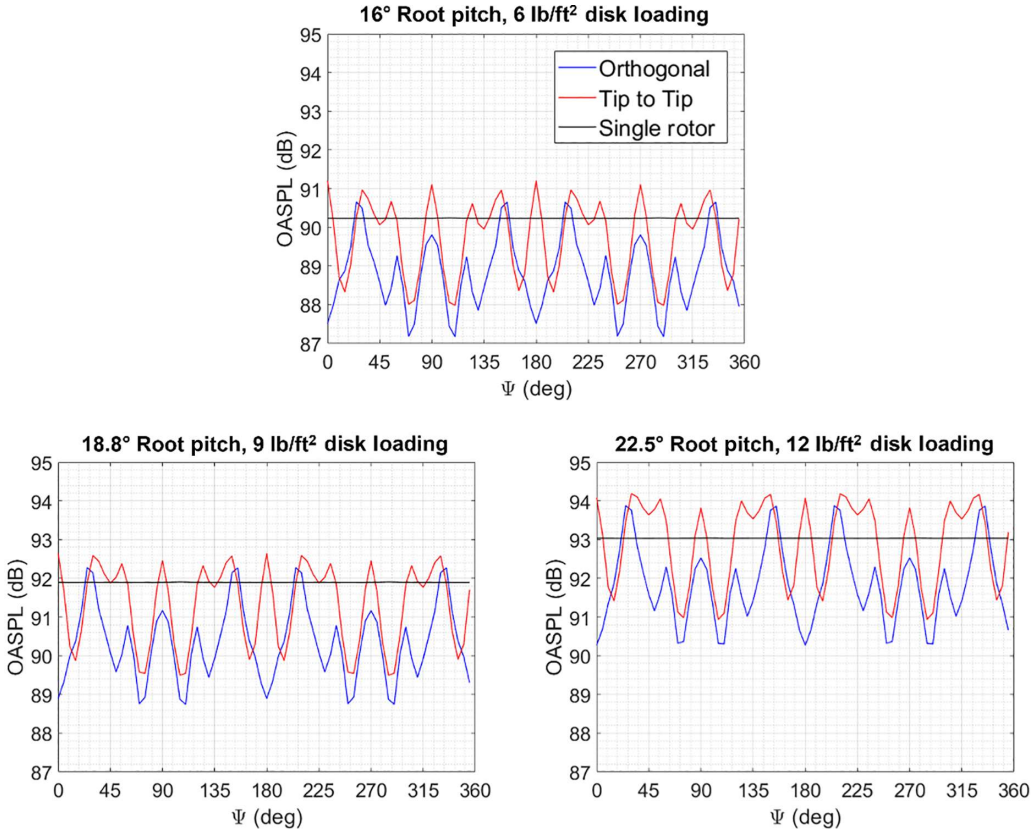

Fig. 26. In-plane OASPL for increasing disk loading with increasing root pitch (constant tip Mach number of 0.6).

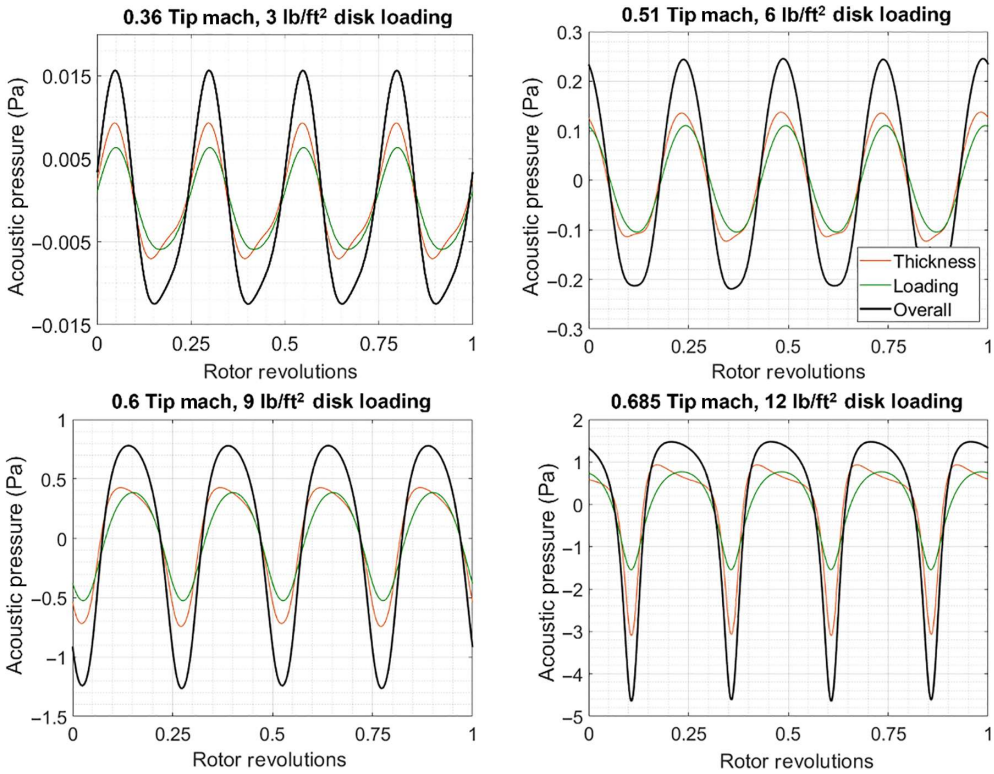

Fig. 27. Acoustic pressure signals, and their decomposition at an in-plane observer along the 90 deg interboom bisector, for increasing disk loading with increasing tip Mach number (constant root pitch of 18.8 deg).

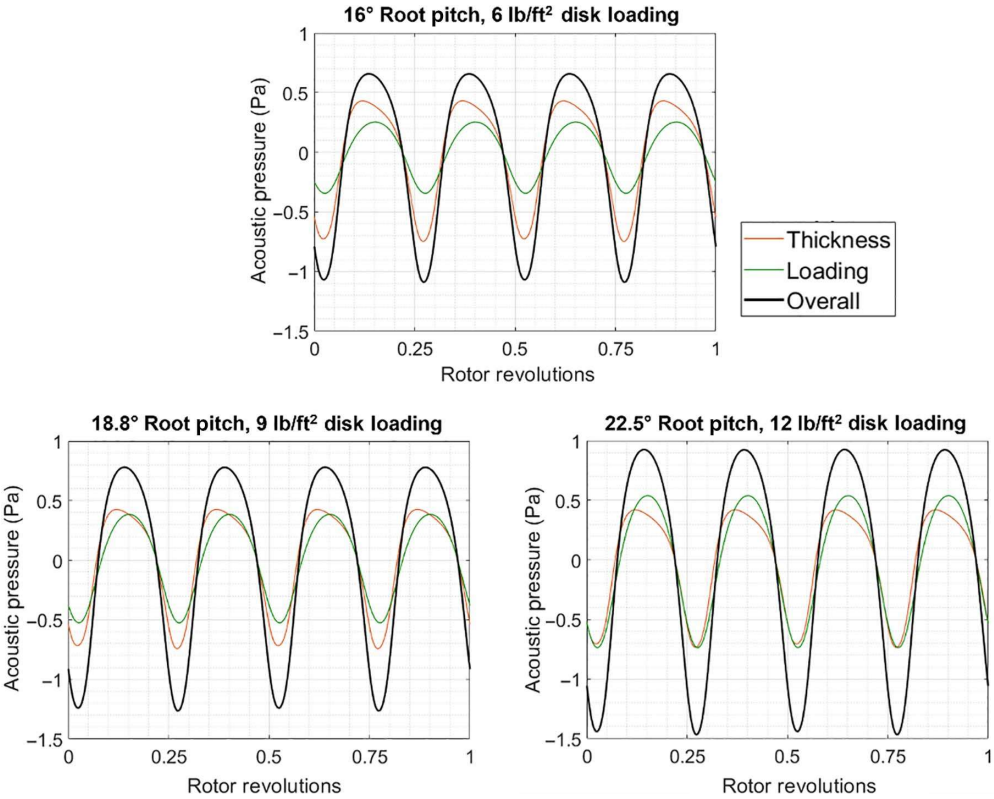

Fig. 28. Acoustic pressure signals, and their decomposition at an in-plane observer along the 90 deg interboom bisector, for increasing disk loading with increasing root pitch (constant tip Mach number of 0.6).

Next, Fig. 26 shows the in-plane OASPL for the points D, B, and E in Fig. 24, with the equivalent single rotor again included for reference. With the tip Mach number held at 0.6, when the disk loading is increased from 6 to 9 to 12 lb/ft^2 by increasing root pitch from 15.9 deg to 18.8 deg to 22.5 deg the single rotor OASPL shows a much smaller 3 dB change, from 90 to 92 to 93 dB. Recall that in comparison, when disk loading was increased over the same range by holding the pitch at 18.8 deg and increasing tip Mach number from 0.51 to 0.685, the single rotor in-plane OASPL increased by 12 dB (from 86 to 98 dB). In Fig. 26, the quadrotor in-plane OASPL levels lie between −3 to +1 dB of the single rotor, for both orthogonal and tip-to-tip phasing, with no evidence of strong noise directionality observed at lower Mach numbers (0.36 and 0.51), even at 6 lb/ft^2 disk loading.

For variation in tip Mach number and disk loading conditions corresponding to points F, A, B, and C, Fig. 27 shows the acoustic pressure signals at an in-plane interboom (90 deg) location, for orthogonal rotor phasing. Also shown in the figure are the thickness and loading noise contributions. While at tip Mach numbers of 0.36, 0.51, and 0.6 (corresponding to disk loading values of 3, 6, and 9 lb/ft^2), the thickness noise is only slightly greater than the loading noise, at a tip Mach number of 0.685 (disk loading of 12 lb/ft^2), the thickness noise starts to dominate and becomes the major contributor to the total noise. For variation in root pitch and disk loading conditions corresponding to points D, B, and E, Figure 28 shows the acoustic pressure signals, and decomposition into contributing sources, at the same observer location, and for the same orthogonal rotor phasing. At tip Mach number 0.6, at lowest pitch (and disk loading), the thickness noise dominates. With the tip Mach number unchanged and root pitch increased to increase disk loading, the loading noise is observed to progressively increase and increases to levels comparable to the thickness noise at 12 lb/ft^2 disk loading.

Conclusions

This study examines the acoustic behavior of manned-size, multirotor, eVTOL aircraft with four, six, and eight rotors (arranged in classical quadcopter, hexacopter, and octocopter configurations) in hover. The rotors were assumed to have collective pitch control and operate at a specified RPM, with the ability to control phasing between the rotors. Two specific phasing scenarios, referred to as orthogonal and tip-to-tip, were considered in the study. The nominal aircraft weight was 1206 lb, and the total rotor disk area and rotor tip speed for all configurations were the same, corresponding to a nominal disk loading of 6 lb/ft^2, and tip Mach number of 0.51. The larger rotors of the quadcopter had a 4-ft radius and nominally operated at 1371 RPM, while the smallest rotors of the octocopter had a 2.83-ft radius and operated at 1939 RPM. The aerodynamic loads on the rotor blades were calculated using the RMAC, and these were provided as inputs to the acoustic propagation code to evaluate the acoustic pressure time history at desired observer locations, considering thickness and loading noise sources from the various rotors. The acoustic pressure histories were in turn used to calculate frequency spectra of sound pressure levels as well as OASPL and radiated acoustic power over an observer hemisphere. The simulation tools used in this study were validated against experimental and simulation results from NASA Langley Research Center and showed good agreement. From the simulations conducted in the present study the following key conclusions can be drawn:

1) For the quadcopter with orthogonal phasing, low-noise regions are observed along the interboom bisectors, with reductions between 5 and 9 dB relative to the equivalent single rotor. No such directivity pattern was evident with tip-to-tip phasing. Differences between the noise lows along orthogonal interboom bisectors were explained by phasing between acoustic signals from different rotor pairs. Despite the noise directivity (or lack thereof), the total radiated acoustic power (PWL) over the observer hemisphere appeared to be comparable between the orthogonal and tip-to-tip phasing cases.

2) For the hexacopter with orthogonal phasing, noise reductions of up to 9.5 dB are observed along alternate interboom bisectors, relative to the equivalent single rotor. A strong directivity pattern was also observed with tip-to-tip phasing. For the octocopter with orthogonal phasing, 13–14 dB noise reductions are observed along interboom bisectors, but like the quadcopter directivity in propagated noise was absent for tip-to-tip phasing. For both the hexacopter and octocopter, orthogonal phasing shows a reduction in total radiated acoustic power (PWL) relative to the equivalent single rotor, while tip-to-tip phasing shows an increase.

3) As the number of rotors increases, an examination of the sound pressure level frequency spectra indicates that the smaller, faster spinning rotors have more tonal peaks at progressively higher frequencies. As a consequence, A-weighting would significantly penalize the smaller, faster-spinning rotors, regardless of orthogonal or tip-to-tip phasing.

4) The effect of change in disk loading on the radiated noise was examined for the quadcopter. When the tip Mach number was increased to achieve higher disk loadings of 9 and 12 lb/ft^2 (while holding the rotor root pitch) the overall noise levels increased significantly and the low-noise regions along the interboom bisectors with orthogonal phasing (previously seen at 6 lb/ft^2) were no longer evident. Conversely, when the tip Mach number was decreased to achieve a disk loading of 3 lb/ft^2 the overall noise levels decreased significantly and the low-noise regions along the interboom bisectors became even more pronounced (with 18–25 dB reductions over the equivalent single rotor). Holding the tip Mach number (at 0.6) and changing disk loading through variation in root pitch had a much smaller effect on radiated noise levels, and quiet regions along interboom bisectors with orthogonal phasing were not observed. Noise directionality with orthogonal phasing (low noise along interboom bisectors) appears strongest when low tip Mach numbers result in a correspondingly lower disk loading.

Acknowledgements

The work carried out at the Rensselaer Polytechnic Institute was funded in part under the Army/Navy/NASA Vertical Lift Research Center of Excellence (VLRCOE) Program, grant number W911W61120012, with Dr. Mahendra Bhagwat as Technical Monitor.

References

[1]Holden, J., and Goel, N., "Fast-Forwarding to a Future of On-Demand Urban Air Transportation," UBER Elevate Whitepaper, October 2016, available at https://prismic-io.s3.amazonaws.com/joby-site/f6fd80b3-da41-41d5-9d00-8f31dfca4c17_Elevate%2BWhitepaper.pdf, accessed October 10, 2019.

[2]NASA, "NASA's UAM Grand Challenge," August 2019, available at https://ntrs.nasa.gov/api/citations/20200001287/downloads/20200001287.pdf, accessed October 10, 2019.

[3]Swartz, K., "NASA Embraces Urban Air Mobility," *Vertiflite Magazine*, January–February 2019, available at: https://evtol.news/news/nasa-embraces-urban-air-mobility, accessed October 10, 2019.

[4]Schmitz, F., "The Challenges and Possibilities of a Truly Quiet Helicopter: 29th Alexander A. Nikolsky Honorary Lecture," *Journal of the American Helicopter Society*, **61**, 041001 (2016), DOI:10.4050/JAHS.61.041001.

[5]Zawodny, N., Boyd, D. D., and Burley, C., "Acoustic Characterization and Prediction of Representative, Small-Scale Rotary-Wing Unmanned Aircraft System Components," Proceedings of the 72nd Annual

Forum of the American Helicopter Society, West Palm Beach, FL, May 17–19, 2016.

[6]Zawodny, N., and Boyd, D. D., "Investigation of Rotor-Airframe Interaction Noise Associated with Small-Scale Rotary-Wing Unmanned Aircraft Systems," *AIAA Journal*, Vol. 65, No. 1, January 2019. DOI: 10.4050/JAHS.65.012007.

[7]Pettingill, N., and Zawodny, N., "Identification and Prediction of Broadband Noise for a Small Quadcopter," Proceedings of the 75th Annual Forum of the Vertical Flight Society, Philadelphia, PA, May 13–16, 2019.

[8]Schiller, N., Pascioni, K., and Zawodny, N., "Tonal Noise Control using Rotor Phase Synchronization," Proceedings of the 75th Annual Forum of the Vertical Flight Society, Philadelphia, PA, May 13–16, 2019.

[9]Pascioni, K. A., Rizzi, S. A., and Schiller, N. H., "Noise Reduction Potential of Phase Control for Distributed Propulsion Vehicles," AIAA 2019-1069, Proceedings of the AIAA SciTech Forum and Exposition, San Diego, CA, January 7–11, 2019.

[10]Thurman, S. C., Zawodny, S. N., Baeder, D. J., "Computational Prediction of Broadband Noise from a Representative Small Unmanned Aerial System Rotor," Proceedings of the 76th Annual Forum of the Vertical Flight Society, Virtual, 5–8, 2020.

[11]Intaratep, N., Alexander, W., and Devenport, W., "Experimental Study of Quadcopter Acoustics and Performance at Static Thrust Conditions," Proceedings of the 22nd AIAA/CEAS Aeroacoustics Conference, Lyon, France, May 30–June 1, 2016.

[12]Tinney, C., and Sirohi, J., "Multirotor Drone Noise at Static Thrust," *AIAA Journal,* Vol. 56, (7), July 2018, pp. 2816-2826, DOI:10.2514/1.J056827.

[13]Tinney, C., and Valdez, J., "Acoustic Scaling for Small Rotors in Hover," Proceedings of the 75th Annual Forum of the Vertical Flight Society, Philadelphia, PA, May 13–16, 2019.

[14]Passe, B., and Baeder, J., "Computational Aeroacoustics of Different Propeller Configurations for eVTOL Applications," Proceedings of the Vertical Flight Society's Autonomous VTOL Technical Meeting and Electric VTOL Symposium, Mesa, AZ, January 29–31, 2019.

[15]Quackenbush, T., Wachspress, D., Moretti, L., Barwey, D., Lewis, R., and Brentner, K., "Aeroacoustic Modeling of an eVTOL Slowed Rotor Winged Compound Aircraft," Proceedings of the 75th Annual Forum of the Vertical Flight Society, Philadelphia, PA, May 13–16, 2019.

[16]Jia, Z. and Lee, S., "Computational Study on Noise of Urban Air Mobility Quadrotor Aircraft," *Journal of the American Helicopter Society*, **67**, 012009 (2022). DOI: 10.4050/JAHS.67.012009.

[17]Wachspress, D., Yu, M., and Brentner, K., "Rotor/Airframe Aeroacoustic Prediction for eVTOL UAM Aircraft," Proceedings of the 75th Annual Forum of the Vertical Flight Society Philadelphia, PA, May 13–16, 2019.

[18]Zhang, J., Brentner, K., and Smith, E., "Prediction of the Aerodynamic and Acoustic Impact of Propeller-Wing Interference," Proceedings of the Vertical Flight Society's Transformative Vertical Flight Forum, San Jose, CA, January 21–23, 2020.

[19]Mukherjee, B., and Brentner, K., "Investigation of Propeller-Wing Interaction Noise and Potential Contribution to eVTOL Noise," Proceedings of the Vertical Flight Society's Transformative Vertical Flight Forum, San Jose, CA, January 21–23, 2020.

[20]Li, S., and Lee, S., "UCD-QuietFly: A New Program to Predict Multi-Rotor eVTOL Broadband Noise" Proceedings of the Vertical Flight Society's Transformative Vertical Flight Forum, San Jose, CA, January 21–23, 2020.

[21]Lee, S., Shlesinger, I., "Coaxial Rotor Broadband Noise Prediction in Hover," Proceedings of the 76th Annual Forum of the Vertical Flight Society, Virtual 5–8, 2020.

[22]Jacobellis, G., Singh, R., Johnson, C., Sirohi, J., McDonald, R., "Experimental and Computational Investigation of Stacked Rotor Acoustics in Hover," *Aerospace Science and Technology*, Vol. 116, September 2021. DOI: 10.1016/j.ast.2021.106847.

[23]Mankbadi, R. R., Afari, S. O., and Golubev, V. V., "Simulations of Broadband Noise of a Small UAV Propeller," Proceedings of AIAA SciTech 2020 Forum, Orlando, FL, January 6–10, 2020, https://doi.org/10.2514/6.2020-1493.

[24]Walter, A., McKay, M., Niemiec, R., Gandhi, F., and Ivler, C., "Handling Qualities Based Assessment of Scalability for Variable-RPM Electric Multi-Rotor Aircraft," Proceedings of the 75th Annual Forum of the Vertical Flight Society, Philadelphia, PA, May 13–16, 2019.

[25]Bahr, M., McKay, M., Niemiec, R., and Gandhi, F., "Performance and Handling Qualities Assessment of Large Variable-RPM Multi-Rotor Aircraft for Urban Air Mobility," Proceedings of the 76th Annual Forum of the Vertical Flight Society, Montreal, Canada, May 2020.

[26]Walter, A., McKay, M., Niemiec, R., Gandhi, F., and Ivler, C., "Handling Qualities of Fixed-Pitch, Variable-RPM Quadcopters of Increasing Size," *Journal of the American Helicopter Society*, **67**, 042010 (2022), DOI:10.4050/JAHS.67.042010.

[27]Niemiec, R., Gandhi, F., Lopez, M., and Tischler, M., "System Identification and Handling Qualities Predictions of an eVTOL Urban Air Mobility Aircraft Using Modern Flight Control Methods," Proceedings of the 76th Annual Forum of the Vertical Flight Society, Virtual 5–8, 2020.

[28]"Joby Aviation Unveils S4." January 2020, available at https://evtol.news/2020/01/15/joby-aviation-unveils-s4, accessed February 10, 2021.

[29]Niemiec, R., Gandhi, F., and Kopyt, N., "Relative Rotor Phasing for Multicopter Vibratory Load Minimization," *The Aeronautical Journal*, Vol. 126, (1298), April 2022, pp. 710–729. DOI:10.1017/aer.2021.94.

[30]Makkar, G., Niemiec, R., and Gandhi, F., "Relative Rotor Phasing for Vibratory Load Minimization for a Coaxial Multicopter," Proceedings of the 78th Vertical Flight Society Annual Forum, Fort Worth, TX, USA, May 10–12, 2022.

[31]Wendelsdorf, J. W., and Berry, L. V., "Method for Suppressing Vibration and Acoustic Signature in a Tiltrotor Aircraft," U.S. Patent No. 8201772B2, U.S. Patent and Trademark Office, 2012.

[32]Bervirt, J., Mikic, G. V., Ryan, J., Stoll, A., Thodal, R., and Bain, J., "System and Method for Aircraft Noise Mitigation," U.S. Patent No. 2021078715A1, U.S. Patent and Trademark Office, 2021.

[33]Niemiec, R. and Gandhi, F., "Development and Validation of the Rensselaer Multicopter Analysis Code (RMAC): A Physics-Based Comprehensive Modeling Tool," Proceedings of the 75th Annual Forum of the Vertical Flight Society, Philadelphia, PA, May 13–16, 2019.

[34]Brentner, K., Bres, G. A., and Perez, G., "Maneuvering Rotorcraft Noise Prediction: A New Code for a New Problem," Proceedings of the AHS Aerodynamics, Acoustics, and Test and Evaluation Technical Specialist Meeting, San Francisco, CA, January 23–25, 2002.

[35]Lopes, V. L., and Burley, C. L, "Design of the Next Generation Aircraft Noise Prediction Program: ANOPP2," Proceedings of the 17th AIAA/CEAS Aeroacoustics Conference, Portland, OR, June 5–6, 2011.